Bolton, M. D. & Stewart, D. I. (1994). *Géotechnique* **44**, No. 1, 111–127

The effect on propped diaphragm walls of rising groundwater in stiff clay

M. D. BOLTON* and D. I. STEWART†

The Paper investigates the stability and serviceability of propped diaphragm walls constructed in situ in stiff clay, first when an excavation is formed in front, second when the groundwater level recovers, and third when it is raised. Three centrifuge model tests were conducted to observe the behaviour of these structures. Simplified behavioural mechanisms are shown to provide a method of analysis for a propped diaphragm wall which would permit a designer to calculate the soil and structural deformations without recourse to expensive and complicated computer-based analyses. The essential conditions are the satisfaction of equilibrium and compatibility requirements, and the ability to use stress-path specific stress–strain data. Where there was little structural displacement, the earth pressures were calculated using a bilinear approximation to the measured stress path of kaolin in one-dimensional swelling.

KEYWORDS: **centrifuge modelling; clays; deformation; *diaphragm and in situ walls*; earth pressure; groundwater.**

L'article étudie la stabilité et la capacité de service de murs diaphragmes étayés, construits dans une argile raide, premièrement lorsqu'une excavation est réalisée devant le mur, deuxièmement lorsque le niveau de la nappe se rétablit et troisièmement lorsque ce niveau est dépassé. Trois essais de modélisation en centrifugeuse ont été mis en oeuvre pour étudier le comportement de ces structures. Des mécanismes simplifiés de comportement sont proposés afin d'obtenir une méthode d'analyse, pour un mur diaphragme étayé, qui permettrait au constructeur de calculer les déformations du sol et de la structure sans avoir recours à des analyses sur ordinateur onéreuses et compliquées. Les conditions majeures portent sur des conditions d'équilibre et de compatibilité ainsi que sur la possibilité d'utiliser les données spécifiques contrainte-déformation du chemin de contrainte. Pour les déplacements structuraux faibles, la pression des terres a été calculée à partir d'une approximation bilinéaire du chemin de contrainte obtenur sur un kaolin lors d'un gonflement unidimensionnel.

INTRODUCTION

The high value of land in many urban areas makes it desirable that the land-use of any given site is maximized. One solution is to use a propped diaphragm wall to support a deep basement. A reinforced concrete diaphragm wall can be cast in situ into a trench that is temporarily held open by bentonite slurry. Once the concrete has gained sufficient strength, the main excavation can proceed with minimal disturbance to the retained soil. When the proposed use of the excavation permits, it is common practice to prop a diaphragm wall at one or more levels. This has the advantage of reducing both the wall penetration required for stability and the displacement of the retained soil caused by excavation. The props can often form part of the permanent structure; possibly the floor slabs in a deep basement, the roof beam in a cut-and-cover tunnel, or even part of the carriageway in a road cutting.

Many urban areas in the UK are situated on heavily overconsolidated clays, posing a number of potential difficulties for the designer of a propped diaphragm wall. CIRIA Report 104 (Padfield & Mair, 1984), which is often used for the design of diphragm walls in the UK, offers design guidance in terms of ultimate limit states and suitable safety factors, but could not specify pressure distributions applicable to serviceability limit states. The deformations required for stiff clay to reach an ultimate limit state may be too large for the retaining wall to be considered serviceable, certainly when the wall is well propped. Also, the factors of safety employed against collapse may mean that the stresses in service differ greatly from those assumed.

It has been observed that the groundwater levels in many urban areas and notably in London (Simpson, Blower, Craig & Wilkinson, 1989) have been rising because of reduced industrial extraction of water from underlying aquifers. Increases in pore-water pressures in stiff clay near a retaining wall may also be caused by water

Manuscript received 14 May 1992; revised manuscript accepted 10 May 1993.
Discussion on this Paper closes 1 July 1994; for further details see p. ii.
* University of Cambridge.
† University of Leeds.

leaking from damaged water mains or sewers. This has led to concern about the performance of retaining structures in stiff clay subject to swelling. Clay swelling has the potential to cause undesired wall movements or, if such movements are resisted by a retaining wall, structural distress.

Centrifuge tests that modelled diaphragm walls propped at excavation level are reported in this Paper. A shallow penetration model (DWC20) was used to investigate the effects of wall movement: on excavation the wall rotated about the prop, the top of the wall moving towards the excavation. The other two centrifuge tests (DWC21 and SSI01) modelled deeper penetration walls subject to long-term swelling. These walls were unable to rotate, and therefore were representative of any well-propped diaphragm wall subject to rising groundwater.

THE CENTRIFUGE MODEL TESTS

It can be shown that when a model geometrically similar to a field-scale structure is made at a scale $1:n$ and tested at a constant acceleration equivalent to n gravities, the self-weight stress distribution will be correctly modelled if the boundary conditions are also similar (Schofield, 1980). An advantage of centrifuge modelling is that the time taken for both transient and steady-state seepage is reduced by a factor of $1/n^2$ from full scale; one day testing at $125g$ represents nearly 50 years in the field. Thus, a centrifuge model is the only practical way to observe the long-term behaviour of structures in stiff clay.

The dimensions and stiffnesses of the retaining walls and supports were chosen to be broadly consistent with full-scale structures when appropriate scaling factors are applied. Table 1 sets out these details at both model and prototype scale for tests DWC20 and 21 and SSI01. Each prototype wall retained a 10 m face of clay, and was propped at the final level of the excavation. The prototype wall penetration beneath that level increased from 2 m in DWC20 to 5 m in DWC21 and to 10 m in SSI01. The wall bending stiffness in DWC20 was made very large in order to verify the mode of deformation as one of rotation about the prop. The walls in DWC21 and SSI01 were made to model more typical diaphragm wall stiffnesses. The selected prop stiffnesses were sufficient to ensure that their axial compression remained much smaller than the maximum soil displacements observed in the tests.

It was desired that the soil models should deform in conditions of plane strain, so ideally the boundaries parallel to the plane of movement of the model (the front window and the back plate) should be rigid and frictionless. The strong-box used for these model tests was developed and described by Powrie (1986). The front is made from 80 mm thick Perspex so that the centrifuge model can be viewed and photographed during testing; the back is made from 20 mm thick Dural stiffened by cross-beams. The front window and the backplate were well lubricated before the soil models were inserted (Stewart, 1990). Powrie (1986) reported coefficients of friction in the range 0·01–0·02 for these kaolin–grease–solid interfaces tested in direct shear.

A liner of the type first employed by Avgherinos (1969) is used with this strong-box. This liner (of internal dimensions 736 × 257 × 152 mm) is common to a consolidation press, so the soil can be pre-consolidated before centrifuging. The liner seals against the front and back of the centrifuge strong-box, preventing leakage of water from the soil model.

A clay slurry was prepared by mixing kaolin powder with deionized water under a partial vacuum, at a moisture content of 120%. It was then placed in the liner within the consolidation press, and one-dimensionally consolidated to a vertical effective stress of 1200 kPa in increments. The sample was then unloaded in vertical stress decrements of about 100 kPa. The final vertical effective stress in the consolidometer was selected

Table 1. Wall and support details

	Excavated height: m	Penetration: m	Bending stiffness EI: kNm^2/m	Prop stiffness λ: MN/m per m
DWC20				
Model	0·08	0·016	5	158
Prototype	10	2	10^7	158
DWC21				
Model	0·08	0·04	0·6	158
Prototype	10	5	$1·2 \times 10^6$	158
SSI01				
Model	0·08	0·08	0·6	79
Prototype	10	10	$1·2 \times 10^6$	79

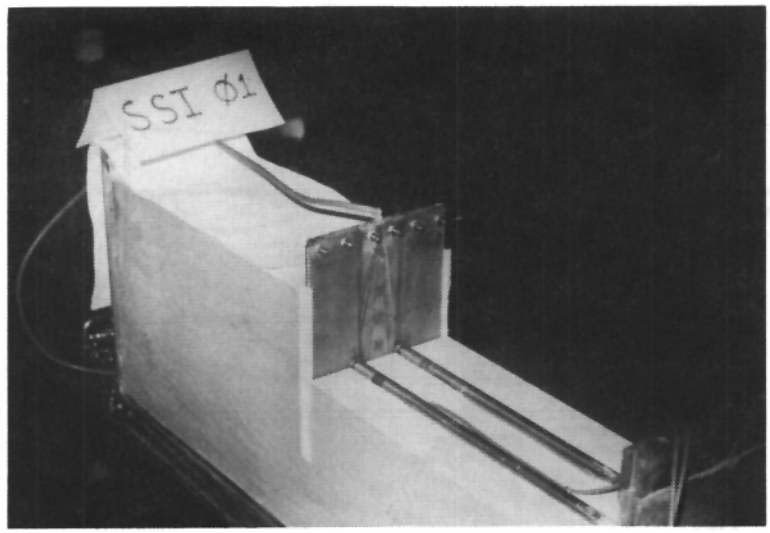

Fig. 1. Model

to be of the same order as the maximum effective stress anticipated in the soil near the model wall just before excavation in the centrifuge test (80 kPa in test DWC20; 400 kPa in tests DWC21 and SSI01 on deeper walls). This ensured that the clay would swell slightly during centrifuge reconsolidation in an attempt to make good contact with the centrifuge strong-box, and to initialize the strain path direction correctly.

The sample was denied access to water before its removal from the consolidation press. The clay was shaped to accommodate the wall and the props, which were then inserted. At this stage clay was removed from the area representing the model excavation, and replaced with a latex rubber bag which was later filled with a dense liquid (zinc chloride). Fig. 1 shows the model at this stage. Excavation was simulated during the centrifuge tests by operating a valve that allowed the zinc chloride solution to drain from the excavation. The zinc chloride solution was mixed to the same density as the clay it replaced, so that

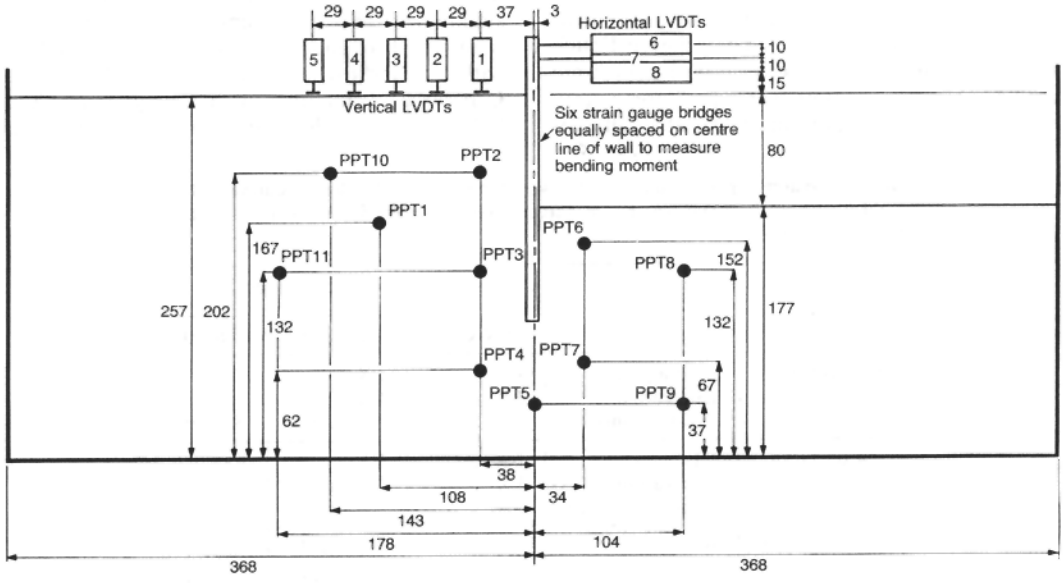

Fig. 2. Instrumentation (dimensions in mm)

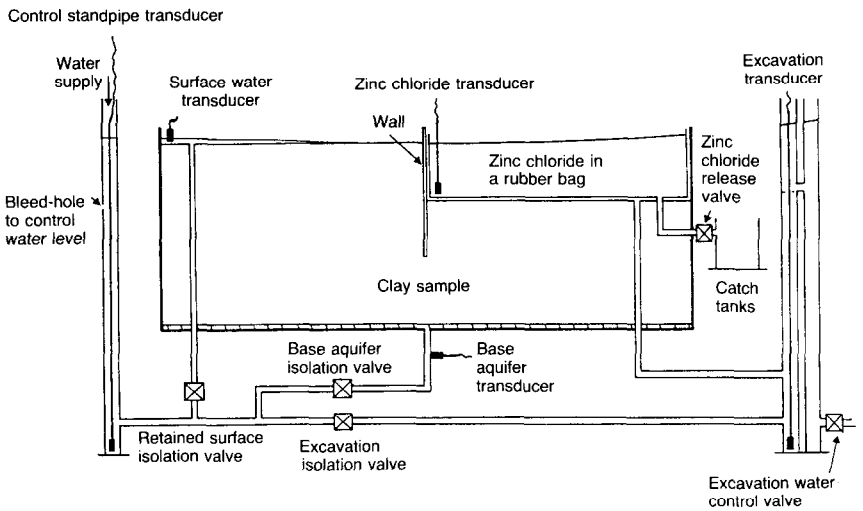

Fig. 3. Fluid control system

the boundary condition imposed on the model walls before excavation would have been approximately equivalent to an earth pressure coefficient of unity in the soil it was supposed to represent (Bolton, Britto, Powrie & White, 1989).

Prior to any construction activity the earth pressure coefficient in a stiff clay is usually greater than 1 and may be 3 or greater, but the slurry trench phase of diaphragm wall construction reduces the coefficient to approximately unity (Powrie, 1985; Tedd, Chard, Charles & Symons, 1984). Thus, the start of the centrifuge tests represented the stage of diaphragm wall construction after the slurry trench phase.

Figure 2 shows the position of the instrumentation within the centrifuge model. Eleven Druck PDCR81 miniature pressure transducers were used to measure the pore-water pressures within the centrifuge models, five linear variable differential transformers (LVDTs) were used to measure movements of the clay surface, three triangulated LVDTs measured wall movements, six full strain gauge bridges (equally spaced on the centre line of the wall) measured wall bending moments, and a full strain gauge bridge measured the force on each prop. Each strain bridge output was amplified by a factor of 100 on the centrifuge arm.

Figure 3 shows how the fluids were controlled during centrifuging. Before testing, zinc chloride solution was placed in the rubber bag, and in a top-up tank which was used to control the level during reconsolidation in the centrifuge. Water levels at the model boundaries were controlled by standpipes. When a single water level was required throughout a model test, a standpipe with an overflow at the required level was used. Otherwise, a standpipe with a very small bleed-hole was used; the height of the water in the

Table 2. Water supply conditions: RS = water supplied at a head equivalent to the height of the retained surface; EX = water supplied at a head equivalent to the height of the excavation

		Head of water supply		
		DWC20	DWC21	SSI01
Pre-excavation	Base aquifer	RS	EX	EX
	Excavation	RS	EX	No supply
	Retained surface	RS	No supply	No supply
Post-excavation	Base aquifer	No supply	EX	EX
	Excavation	EX	EX	No supply
	Retained surface	RS	No supply	No supply
Further changes	Base aquifer	—	Increased	Increased
	Excavation	—	No supply	No supply
	Retained surface	—	No supply	No supply

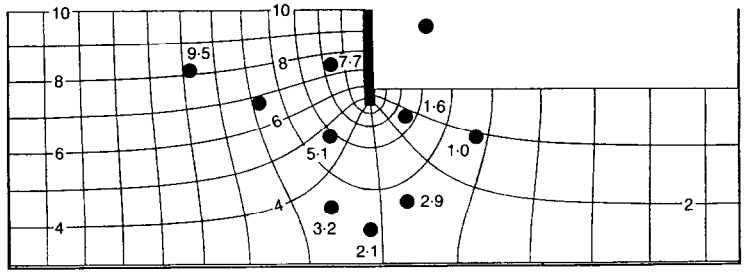

Fig. 4. DWC20 flow net: no curvature correction; numbers shown are potentials in m relative to excavation level

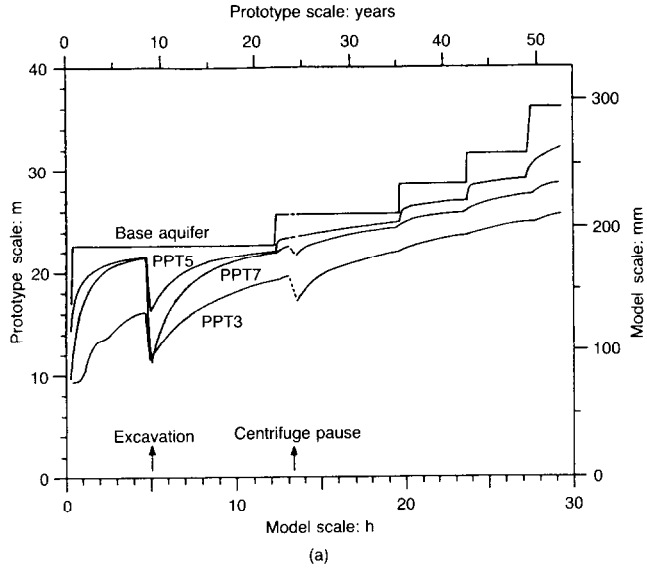

Fig. 5. Rising aquifer potential in models (a) DWC21, (b) SSI01: datum for potential is base of clay, 22 m (prototype) below excavation

standpipe could then be adjusted during a test by alteration of the water supply rate. In general, water could be supplied to three model boundaries: the retained surface, the excavation, and the aquifer underlying the model. Table 2 details how the water was supplied in each test.

The initial water supply conditions in test DWC20 resulted (after a period of reconsolidation) in a water table at the retained soil surface. Immediately before excavation was simulated, the height of the water in the region to be excavated was reduced to the excavation level, and the base aquifer was isolated from the water supply to act as an internal drain. The resulting long-term seepage pattern after excavation is shown in Fig. 4, the internal drain having been observed to achieve a constant potential 3 m above the level of the excavation.

The water supply conditions in tests DWC21 and SSI01 were intended to represent a clay layer overlying a recharging aquifer. During reconsolidation, excavation and subsequent equilibration, water was supplied to the base aquifer at a head equal to excavation base level. The water pressure in the base aquifer was then increased stepwise several times, the models being allowed to approach a steady state between increases. This is illustrated in Fig. 5, which shows the pore-water potential in the base aquifer and at discrete locations within the model during tests DWC21 and SSI01. Without a direct water supply, there was a significant evaporation loss from both the retained surface and the excavation. This was minimized by covering these boundaries with thin rubber sheets, but it still resulted in steady-state upward seepage. This is illustrated in Fig. 6, which shows the long-term seepage pattern after excavation for models DWC21 and SSI01.

ONE-DIMENSIONAL CLAY SWELLING

Figure 7 shows the anticipated stress path in both σ_v'–σ_h' and t–s' plots for clay subjected to a loading–unloading cycle in one-dimensional strain (Schmidt, 1966; Wroth, 1972). At the start of unloading, Wroth (1975) noted an approximate proportionality between the initial changes in vertical and horizontal effective stress in an oedometer, consistent with isotropic elastic rebound at constant Poisson's ratio. As an isotropic stress state was approached, however, the horizontal effective stress started to decrease more sharply, until the decrements of σ_v' and σ_h' were roughly equal and the stress path ran at constant t towards failure at small s'. Wroth (1972) introduced the passive failure criterion as a limit on the stress ratio in one-dimensional swelling. Brooker & Ireland's (1965) data indicate that very high stress ratios $\sigma_h'/\sigma_v' \to \infty$, $t/s' \to -1$ may be achieved at low effective stress levels as a clay

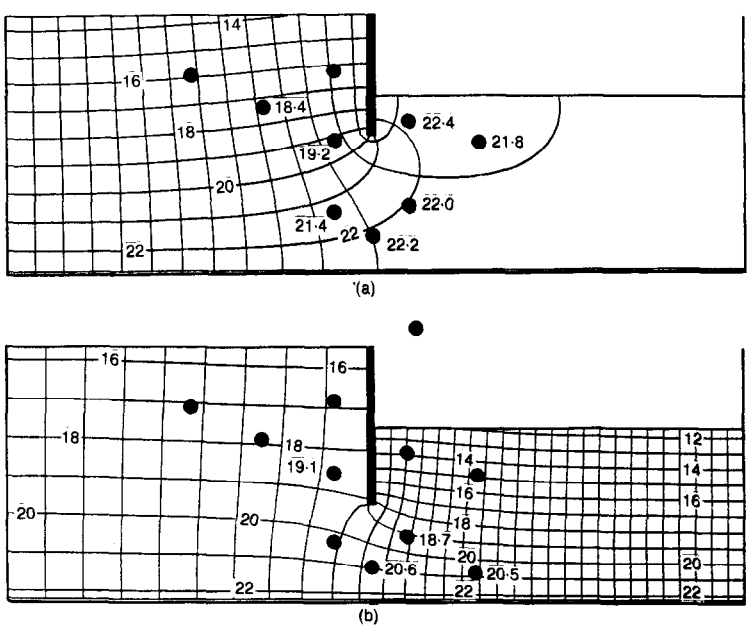

Fig. 6. (a) DWC21 and (b) SSI01 long-term flow nets: no curvature correction; potentials in m (prototype scale) relative to base aquifer level, 22 m below excavation

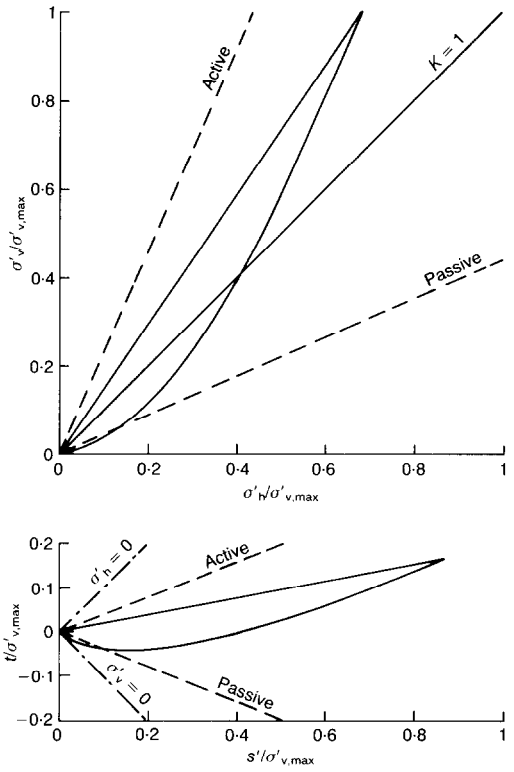

Fig. 7. Stress paths for one-dimensional consolidation and swelling

sample is one-dimensionally unloaded. Burland & Fourie (1985) reported a true cohesion intercept ($c' = \sigma_h'/2$) in the ultimate failure states of undisturbed samples of London Clay subject to complete passive stress relief ($\sigma_v' = 0$), and stress ratios in excess of $\sigma_h'/\sigma_v' \approx 5$, $t/s' \approx -0{\cdot}68$ (corresponding to a secant ϕ of 43°) for reconstituted specimens dilating strongly at failure.

Data from one-dimensional swelling tests (Stewart, 1990) on kaolin, conducted in a strain-path-controlled triaxial apparatus, are typified in Fig. 8. The clay was pre-compressed one-dimensionally to $\sigma'_{v,max} = 1200$ kPa, unloaded in decrements, sampled, and then set up in the stress-path triaxial apparatus under an isotropic effective stress $s' = 200$ kPa. A bilinear elastic–plastic relation has been fitted to the data of subsequent one-dimensional swelling. The initial phase of unloading is bounded by a line of slope 1 on the (t, s') diagram. This is, by definition, a line of constant horizontal effective stress. An elastic interpretation of this response would be of drained unloading with zero Poisson's ratio. Similarly, if this path were the result of a pore-pressure increase under constant vertical total stress, the horizontal effective stress would

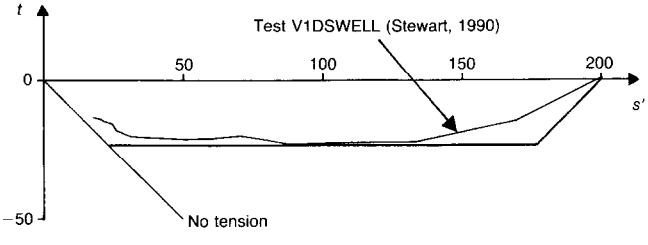

Fig. 8. Stress path data for one-dimensional swelling of kaolin

equally remain constant, so that the horizontal total stress would increase by an amount equal to the increase in pore pressure.

The subsequent plastic behaviour is bounded by a line $t = -c_s$. A line of zero slope on the (t, s') diagram corresponds to zero change in shear stress. If a clay deposit were swelling one-dimensionally due to an increase in the pore-water pressure without a change in the vertical total stress, the horizontal total stress would not be changing in this second stage. The data indicate that samples of overconsolidated kaolin clay continue to support a significant deviatoric stress when the vertical effective stress reduces monotonically to zero, at which tensile cracking must be expected. After monotonic swelling, the magnitude of shear stress eventually developed could be expressed as $c_s \approx 0{\cdot}04\sigma'_{v\,max}$. An extra shearing cycle, as experienced by the centrifuge samples during model preparation, was found to lead to a reduction to $c_s \approx 0{\cdot}02\sigma'_{v\,max}$ (see Fig. 8). When samples were continually subjected to cycles of stress-reversal while swelling, however, failure occurred by shearing at a critical state stress ratio ($t/s' = \sin \phi_{crit} = 0{\cdot}38$).

Fitting of the bilinear approximation on the lower bound of the data in Fig. 8 overestimates the lateral swelling pressure. This overestimate is conservative for the purposes of checking structural serviceability. Stewart (1990) showed that clay swelling in conditions where the radial strain rate was small compared with the axial strain rate followed an unloading stress path very similar to the one-dimensional swelling stress path. Therefore it is thought that the idealized bilinear stress path is applicable to clay swelling near substructures when structural movements are positively restrained.

ANALYSIS OF A SHALLOW PENETRATION WALL PROPPED AT EXCAVATION LEVEL

Test DWC20 indicated that a shallow penetration diaphragm wall propped at excavation level (penetration 20% of excavation depth) would exhibit significant rotation about the prop immediately on excavation, and would become even more unserviceable in the long term. Bolton & Powrie (1988) have shown that statically admissible plastic stress fields and kinematically admissible plastic deformation mechanisms can be used to check the status of walls rotating about either their crest or their toe. An analysis is now performed which uses a similar geostructural mechanism for a wall rotating about a prop at excavation level.

Statically admissible stress fields for the collapse of a structure usually assume a constant soil strength (characterized by either an undrained strength c_u or an angle of shearing resistance ϕ). Bolton & Powrie (1988) propose that similar stress fields are applicable before collapse, but based on mobilization of a constant proportion of the ultimate strength. This, they suggest, will be a significant error only if the stress field before failure varies substantially from that at collapse. They propose that serviceability criteria can be checked by the linking of mobilized shear strength and shear strain using data of plastic hardening obtained from appropriate element tests. The compatible wall displacement can then be inferred from a kinematically admissible strain field.

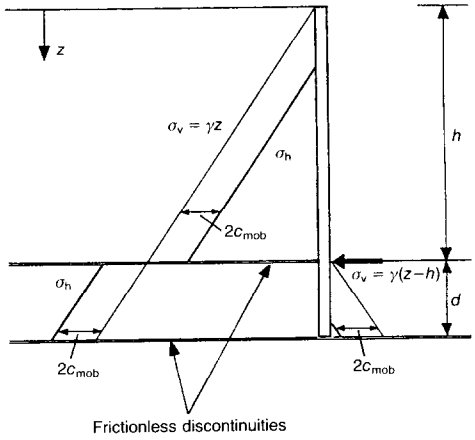

Fig. 9. Equilibrium stress field for wall propped at excavation base: undrained soil

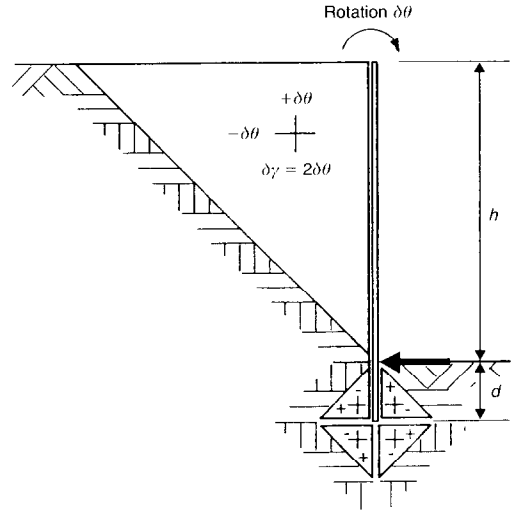

Fig. 10. Kinematically admissible strain field for wall propped at excavation base: undrained soil

Undrained analysis

The statically admissible stress field and the kinematically admissible strain mechanism, shown in Figs 9 and 10 respectively, form a geostructural mechanism for the analysis of a shallow penetration diaphragm wall propped at excavation level. In regions of deformation, the principal stress and strain directions are horizontal and vertical, and the major stress and strain directions everywhere coincide. Strictly, this applies only to a frictionless wall. The mechanism assumes that there is a single shear strain in all regions of (undrained) deformation as the supposedly rigid wall rotates about the prop, into the excavation. If the mobilized strength before excavation is zero (corresponding to $K_0 = 1$), and variations in soil stiffness are ignored, a unique shear strain should mobilize a unique shear strength.

Wroth (1984) suggested an approximate relation of undrained strength ratio (c_u/σ_v') and overconsolidation ratio (OCR = $\sigma'_{v\,max}/\sigma_v'$)

$$c_u/\sigma_v' = a\ \mathrm{OCR}^b \qquad (1)$$

where a and b are constants. Fig. 11 shows undrained strength data for kaolin tested in two different apparatus, plotted on logarithmic axes as undrained strength ratio against OCR. Amerasinge's (1973) data are for Spestone kaolin, the other data are for Speswhite kaolin; but this is not considered significant (Mair, 1979). A linear regression analysis was performed on all the data in Fig. 11. The intercept and slope of the regression line gives values for a and b in equation (1)

$$(c_u/\sigma_v') = 0{\cdot}29\ \mathrm{OCR}^{0{\cdot}405} \qquad (2)$$

Fig. 11 also shows the 95% confidence limits for the central tendency. Fig. 12 shows the estimated

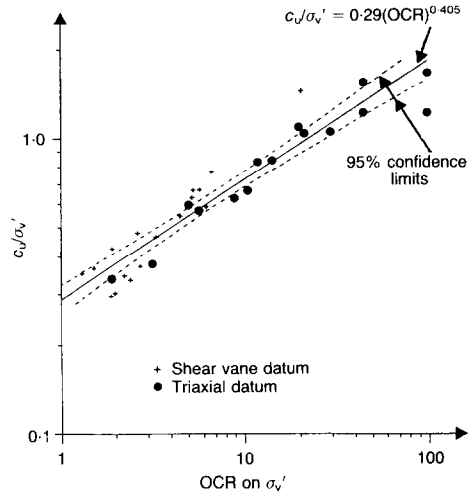

Fig. 11. Undrained strength correlation with OCR: data from Amerasinge (1973), Phillips (1986), Al Tabbaa (1988), Stewart (1990)

undrained strength profile for model DWC20 based on equation (2). The proposed geostructural mechanism assumes that undrained strength is constant with varying depth, therefore the undrained strength profile is averaged over the depth of the wall, to give an undrained strength $c_{u,\,av}$ of 46 kPa within predicted bounds 42 kPa $< c_{u,\,av} <$ 50 kPa.

Equilibrium of the stress field shown in Fig. 9 for model DWC20 would require a mobilized soil strength of 38 kPa provided the tension crack at the soil–wall interface remained dry. If sufficient water were available to fill this tension crack, a mobilized soil strength of about 300 kPa would be required for wall stability; this would have

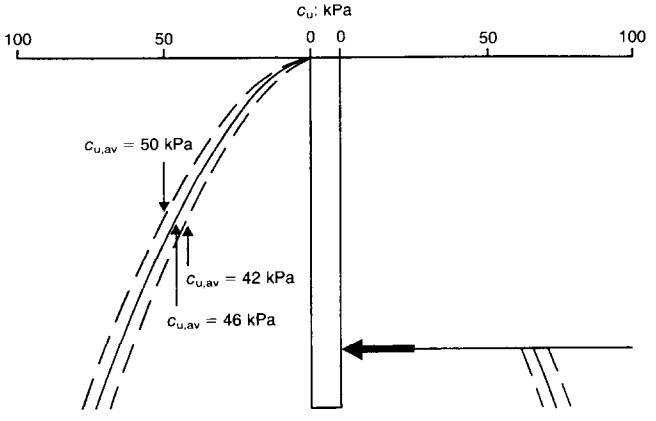

Fig. 12. Undrained strength profile for DWC20

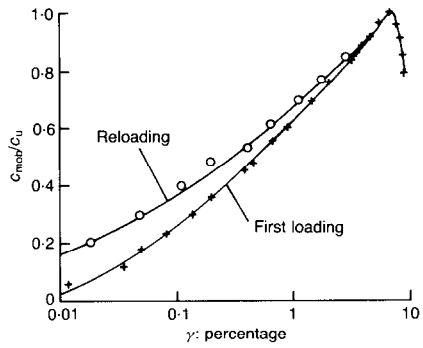

Fig. 13. Plane-strain compression data for kaolin at OCR = 10

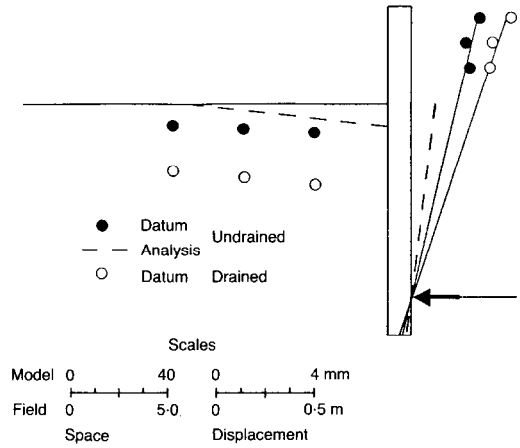

Fig. 14. Immediate and long-term boundary displacements for DWC20

resulted in wall collapse. As the model was stable immediately after excavation, it is inferred that any tension crack was dry.

Also, equilibrium of the stress field shown in Fig. 9 would require a prop force of 0·8 MN/m at field scale (6·4 N/mm at model scale). A prop force of 1·1 MN/m at field scale (8·5 N/mm at model scale) was measured immediately after excavation during the centrifuge model test. Therefore, the proposed geostructural mechanism estimates the wall propping force to be about 75% of that measured. This agreement is satisfactory considering the assumptions that are made about the stress field.

The stress-path data shown in Fig. 13 were used in the deformation analysis of centrifuge model DWC20. This relation, measured by Powrie (1986) in an undrained plane-strain test, is representative of the soil just below wall toe level. The proportion of undrained strength (c_{mob}/c_u) required for wall equilibrium is 0·83, with prediction bounds $0·76 < c_{mob}/c_u < 0·91$. Therefore, the estimated soil shear strain γ is 2·4%, with prediction bounds $\gamma = 1·6\%$ and 4·3%. The shear-strain mechanism shown in Fig. 10 would estimate a wall rotation of 0·012, with prediction bounds of 0·008 and 0·022. The measured wall rotation immediately after excavation was 0·023. Therefore, the best estimate of wall rotation is an underestimate by a factor of 2, but the small uncertainty on undrained strength could explain the shortfall: the stress–strain curve has become quite flat at this high degree of strength mobilization.

Figure 14 compares the undrained boundary displacements calculated for model DWC20 with those measured immediately after excavation during the centrifuge model test. As noted above, the calculated wall rotation is about half of that measured; calculated and measured settlements immediately behind the wall show a similar relation. Photographic film measurement for model DWC20 indicated that retained surface settlement became negligible at a distance of about 16 m prototype scale (130 mm model scale) from the 10 m (80 mm) high wall. The simple plastic deformation mechanism would have underpredicted the width of the settlement trough, setting the limit of influence at 10 m from the wall. It is generally found that linear elastic finite element predictions, on the other hand, significantly overestimate the zone of influence (Hubbard, Potts, Miller & Burland, 1984; Jardine, Potts, Fourie & Burland, 1986).

Drained analysis

In the long term, the wall came into equilibrium (see Fig. 14) with pore-water pressures dictated by the pattern of seepage shown in Fig. 4: these pressures were linearized against depth for calculation purposes. The consequent increase in effective stress throughout the depth of the clay was partly responsible for the relatively large long-term settlement on the retained side. The sharp changes of horizontal effective stress near the toe, due to the reversal of strain direction about the prop and to the reduction of vertical effective stress owing to upward seepage beneath the excavation, lead to difficulties in analysis. Milligan & Bransby (1976), dealing with a similar configuration in dense sand, showed that the passive support on the retained side beneath a pivot could be very large, especially when wall friction could be developed. They showed experimentally that the passive resultant acted close to the base of the wall. Fig. 15 shows the predicted state of drained equilibrium for DWC20 based on the achievement of fully active conditions above the prop ($\phi_{max} = 29·5°$ at OCR = 20) (Stewart,

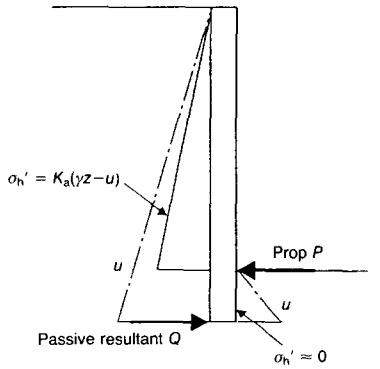

Fig. 15. Drained equilibrium stresses and forces for DWC20

1990). The effective stress component of the passive support force is taken at the base; the effective active pressure beneath the excavation is ignored. Moment equilibrium about the base now dictates that the propping force should be 1·36 MN/m (10·9 N/mm at model scale). This compares well to the value of 1·2 MN/m (9·2 N/mm) obtained from the model test.

ANALYSIS OF DEEP PENETRATION WALLS PROPPED AT EXCAVATION LEVEL

When excavation was performed in model tests DWC21 and SSI01, the immediate wall movements were very small. These wall movements were insufficient even to bring the walls into effective contact with the wall props, but load cells in the wall props indicated that the walls were effectively propped very shortly after excavation. If a field-scale diaphragm wall were to be propped at excavation base level, the excavation would have to proceed (at least partially) before the wall props could be constructed. In such circumstances, the wall would either require temporary shoring or have to rely on the undrained strength of the soil for support: even unsupported excavations in stiff clay can be stable before drainage occurs. The centrifuge model tests were representative of the situation.

Construction of the excavation

The movements of an unpropped rigid wall immediately on excavation are thought to be characterized well but the shear-strain mechanism shown in Fig. 16 (Bolton, Powrie & Symons, 1990), in which all regions of soil deformation undergo the same shear strain. If the original earth pressure coefficient in the wall vicinity was approximately unity and accepting that the pore-water pressure boundary conditions of models DWC21 and SSI01 resulted in an approximately uniform OCR throughout, a single shear strain in regions of soil deformation might be assumed—as a first approximation—to mobilize a single soil strength $c_{mob} = c_i$ due to excavation.

Bolton, Powrie & Stewart (1987) presented the stress field shown in Fig. 17 for an unpropped rigid diaphragm wall embedded in stiff clay. The equilibrium diagram assumes conditions of fixed earth support: this is accurate enough since the point of rotation can be shown to lie very close to the base (Bolton *et al.*, 1990). The mobilized soil strength and the force Q are then found by considering moment and horizontal force equilibrium.

Before excavation, the stress state at a general point R in the retained soil behind a diaphragm wall can be represented by points R_0 and R_0' in Fig. 18 (the pore-water pressure at point R has arbitrarily been taken as negative). If it is assumed that the surface of the retaining wall is frictionless, on excavation there will be no change

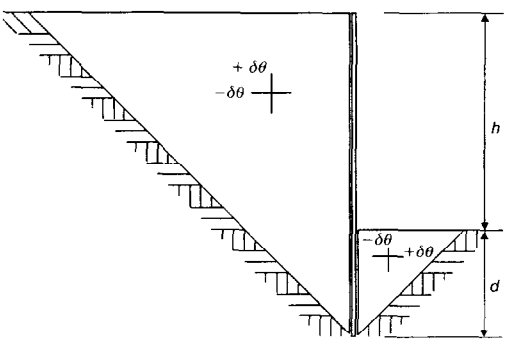

Fig. 16. Kinematically admissible strain field for a free cantilever in undrained soil

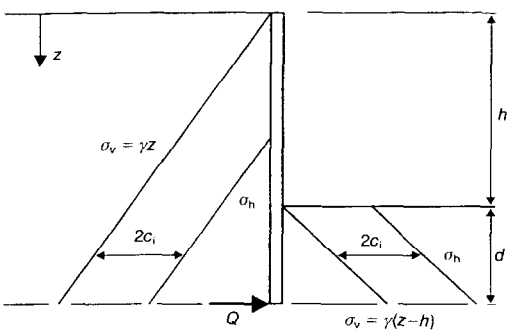

Fig. 17. Approximate equilibrium for undrained excavation against a free cantilever

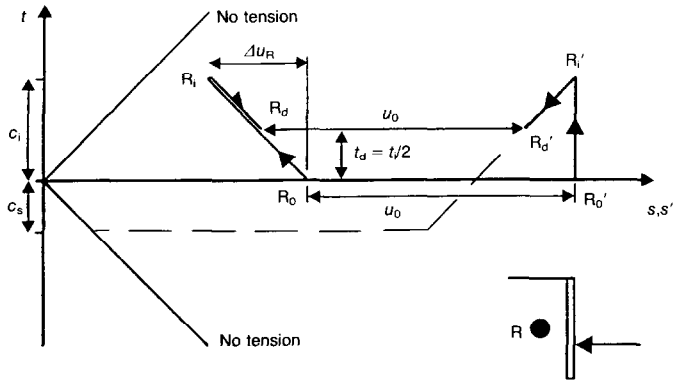

Fig. 18. Stress path at and after excavation: retained soil

in the vertical total stress in the retained soil. Therefore the total stress state immediately after excavation will be indicated by point R_i mobilizing a shear stress $t = c_i$, where $R_0 R_i$ is a straight line of gradient -1 in t–s space. The horizontal total stress acting on the retained side of the wall at the end of excavation will therefore be

$$\sigma_h = \sigma_v - 2c_i \tag{3}$$

The effective stress path $R_0' R_i'$, however, will be approximately perpendicular to the s' axis, as shown, because the clay will deform quasi-elastically at constant volume.

Before excavation, the stress state at a general point E in the soil beneath the excavation can be represented by points E_0 and E_0' in Fig. 19. On excavation, the effective stress path $E_0' E_i'$ will also be approximately perpendicular to the s' axis, and will also reach a shear stress equal in magnitude to c_i. Therefore the horizontal total stress acting on the excavation side of the wall at the end of excavation is

$$\sigma_h = \sigma_v + 2c_i \tag{4}$$

The total stress path for point E during excavation can be deduced from the stability of a partially formed excavation in the same way.

During transient drainage

At the end of excavation there will be a negative excess pore-water pressure in the retained clay ($\Delta u_R = -c_i$ in Fig. 18), because during excavation there is a reduction in the average total stress s without a reduction in the average effective stress s'. As already stated, this excess pore-water pressure must dissipate in conditions of virtually no horizontal strain. Therefore, the effective stress path is assumed to follow the idealized one-dimensional elastic swelling stress path, and the excess pore-water pressure will dissipate without change in the horizontal effective stress. Thus, the idealized effective stress path will follow a line of slope $+1$ in Fig. 18, while the total stress

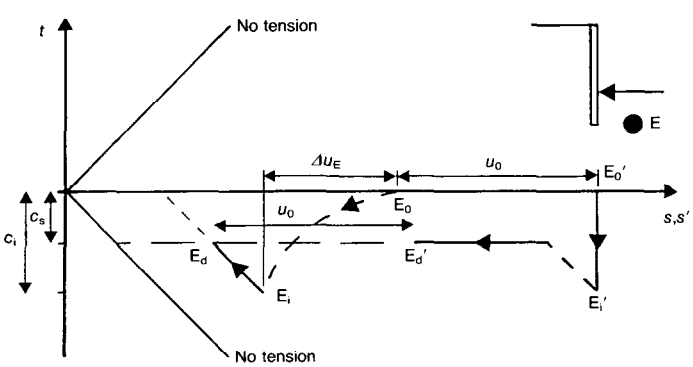

Fig. 19. Stress path at and after excavation: soil beneath excavation

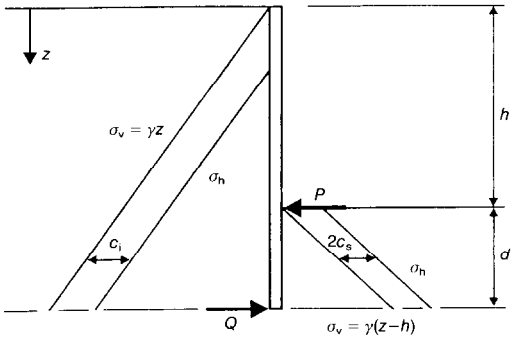

Fig. 20. Approximate drained earth pressure distribution

path must have a slope of -1 since vertical total stress is constant. Therefore both the total and effective stress states (R_d and R_d' in Fig. 18) can be obtained, and it will be seen that the shear stress $t_d = c_i/2$. The horizontal total stress acting on the retained side of the wall at this stage is therefore

$$\sigma_h = \sigma_v - 2t_d = \sigma_v - c_i \quad (5)$$

A similar argument can be used to deduce the long-term stress state at the general point E in the soil beneath the excavation. Once the excavation is complete, there will be no further change in the vertical total stress (assuming no wall friction). Thus the total stress path must remain on a line in t–s space of gradient -1. Excavation will have induced a negative excess pore-water pressure at point E (Δu_E in Fig. 19). The effective stress path is assumed to follow the idealized one-dimensional swelling stress path as this excess pore-water pressure dissipates, and so the total and effective stress states after dissipation of transient pore-water pressures will be E_d and E_d'.

Any reasonable excavation depth will result in sufficient stress relief to ensure that point E_d' is on the constant t portion of the idealized swelling stress path. Therefore the horizontal total stress acting on the excavation side of the wall after the transient pore-water pressures have dissipated is

$$\sigma_h = \sigma_v + 2c_s \quad (6)$$

If the shear stress c_i required for undrained wall stability immediately after excavation is greater than c_s, then it is assumed that the effective stress path will move back on to the idealized one-dimensional swelling stress path during pore-water pressure dissipation.

The idealized earth pressure distribution in the long term after excavation is shown in Fig. 20. A negative prop force P or a large toe force Q would indicate that the one-dimensional swelling assumption made above is inappropriate to the case under study due to a tendency towards wall rotation.

Swelling due to rising groundwater level

Increasing the groundwater level in the centrifuge tests did not result in any accumulation of surface water, either at the retained surface or in the excavation. Therefore, assuming no wall friction, there will be no change in the vertical total stress. So, at the general point R in the retained soil, the total stress path will remain on the line of gradient -1, shown in Fig. 21. The effective stress path will follow the idealized one-dimensional swelling path until the difference between the average total stress s and the average effective stress s' has reduced by an amount equal to the pore pressure rise Δu_s (see Fig. 21), and hence the idealized total and effective stress paths for point R will reach R_s and R_s' respectively. At this stage the horizontal total stress acting on the retained side of the wall will be

$$\sigma_h = \sigma_v - c_i + \Delta u_s \quad (7)$$

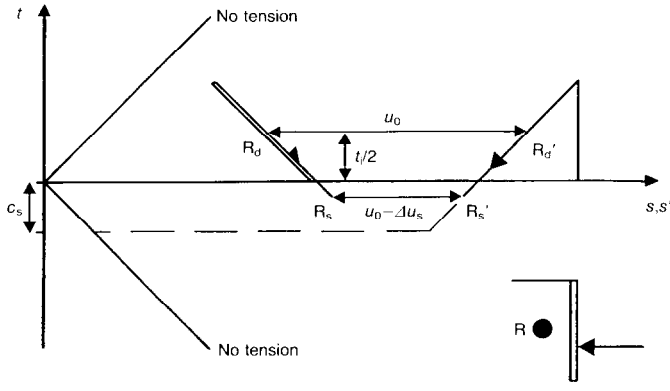

Fig. 21. Stress path for rising groundwater: retained soil

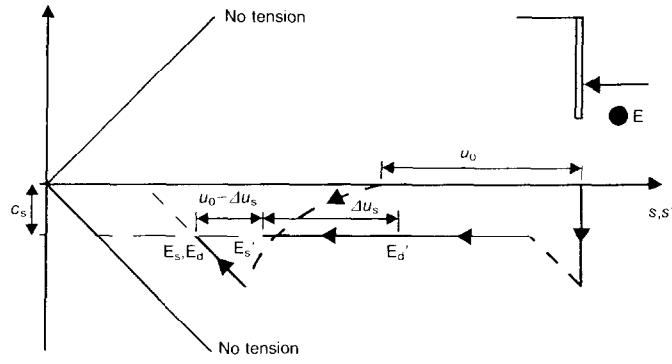

Fig. 22. Stress path for rising groundwater: soil beneath excavation

but the assumption of the bilinear one-dimensional swelling stress path will impose a limit on the horizontal total stress of

$$\sigma_h = \sigma_v + 2c_s \quad (8)$$

Similar reasoning can be used to deduce the idealized total and effective stress paths for the general point E beneath the excavation. As the effective stress path is already following the constant shear stress portion of the idealized one-dimensional swelling response, the horizontal total stress in the soil beneath the excavation will not change, so equation (8) also applies. Therefore the average effective stress s' will reduce by an amount equal to Δu_s, and the total and effective stresses at a general point E in the soil beneath the excavation will be represented by points E_s and E_s' in Fig. 22.

The idealized earth pressure distribution after an increase in groundwater level is shown in Fig. 23. Again, a negative prop force P or a large toe force Q would indicate that the assumptions were inappropriate in the specific case.

Comparison of the analysis with the centrifuge model tests

During the centrifuge tests, the water pressure in the base aquifer was increased incrementally, and each water-pressure increment was followed by a period of observation to study the influence of that particular increment on the model behaviour. The analysis does not consider transient flow, therefore the points of comparison of the analysis and the centrifuge model tests are

(*a*) immediately after excavation: this analysis is undrained; excavation occurred slowly in model test SSI01 so no comparison is available for that test

(*b*) at the end of the observation period of transient flow after excavation

(*c*) at the end of the observation period after the final increase in base aquifer potential: the increase in pore-water pressure in the vicinity of the model walls was less than the increase in the base aquifer water pressure because of surface evaporation, therefore transducer PPT3 was used to estimate the pore-pressure increase near the model wall (see Figs 2 and 5).

The undrained strength profiles of models DWC21 and SSI01 have been estimated by use of equation (2). In both models, the undrained strength immediately before excavation was approximately constant with depth; $c_{u,av}$ was 122 kPa in test DWC21 and 135 kPa in test SSI01. On excavation, it is calculated that model DWC21 mobilized a strength of 57 kPa, and model SSI01 52 kPa. Once a steady state was reached after excavation, the pore-water pressure in the wall vicinity was increased by a total of ~65 kPa during test DWC21, and by 80 kPa during test SSI01. The value of c_s was taken to be 23 kPa, using the Fig. 8 data for a swelling test with a single cycle of stress reversal.

Figure 24 compares the wall bending moments

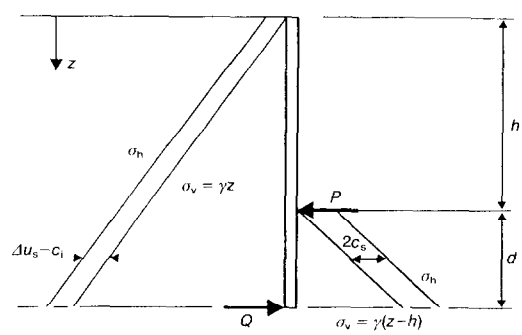

Fig. 23. Approximate swelling pressure distribution

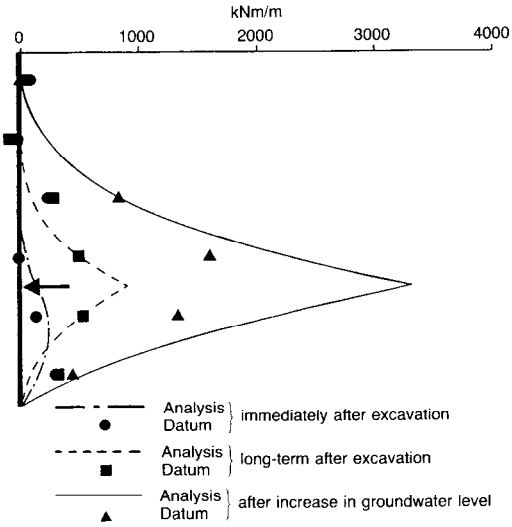

Fig. 24. Bending moments for DWC21

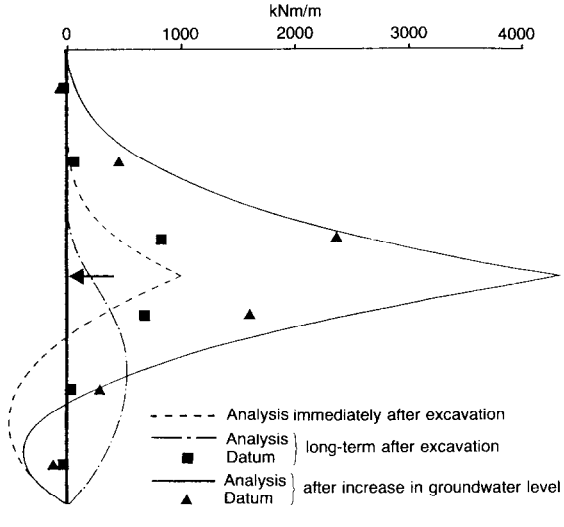

Fig. 25. Bending moments for SSI01

Table 3. Prop forces in DWC21

	Prop force: kN/m		Additional force Q required for equilibrium in analysis: kN/m
	Measured	Calculated	
Immediately on excavation	—	0	157
Long-term after excavation	683	758	−1
After 65 kPa increase in pore-water pressure	1160	1961	321

Table 4. Prop forces in SSI01

	Prop force: kN/m		Additional force Q required for equilibrium in analysis: kN/m
	Measured	Calculated	
Immediately on excavation	—	0	185
Long-term after excavation	872	914	−284
After 80 kPa increase in pore-water pressure	1714	2372	−353

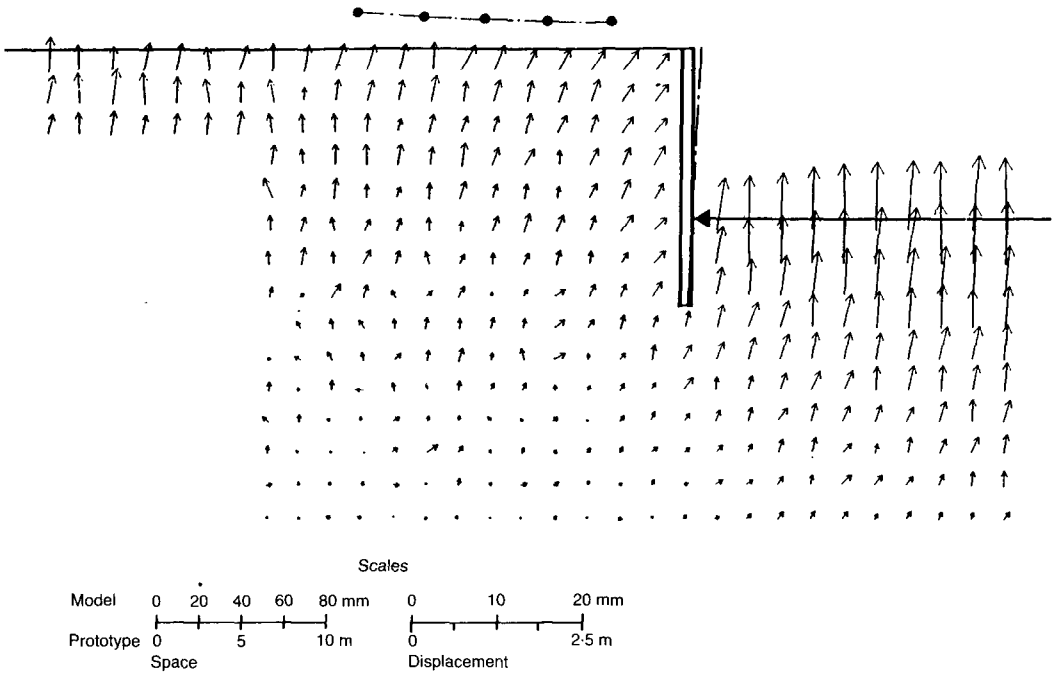

Fig. 26. Displacements of model DWC21 when the pore-water pressure in the base aquifer had been increased by 120 kPa

calculated for model DWC21 with those measured during the centrifuge model test; Table 3 compares the calculated and measured prop forces. Likewise, Fig. 25 and Table 4 compare the analysis with measurements made during centrifuge model test SSI01. As expected, the analysis gives a moderate overestimate of the prop force and the wall bending moments following swelling. The two tests do suggest, however, that a design approach based on these principles will be sufficiently accurate for practical purposes. Fig. 26 shows the final soil displacements following the raising of groundwater pressures in DWC21, confirming that one-dimensional swelling is a sufficiently good representation of long-term soil movements around this well-supported wall.

CONCLUSIONS

Centrifuge model tests allowed the long-term behaviour of a propped diaphragm wall in stiff clay to be observed in a few hours: this would take many years at prototype scale.

Observation of centrifuge model tests was essential in the creating of simplified behavioural mechanisms for analysis. These simplified plastic mechanisms obeyed the conditions of equilibrium and compatibility, with coincidence of principal axes.

The accurate prediction of model behaviour depends entirely on the selection of appropriate stress path tests for soil elements. This work has featured behaviour in swelling clays, and a large programme of swelling strain path tests was conducted. These showed that characterization of this behaviour as elastic is inappropriate, even inside what is normally assumed to be the plastic yield surface.

The stress path followed by kaolin in one-dimensional unloading was idealized as bilinear. This facilitated hand calculations for the horizontal effective stress acting on a deep penetration diaphragm wall propped at excavation level. By fitting of the bilinear approximation below the test data on a $t:s'$ diagram, the horizontal lateral stress will be overestimated: this procedure is conservative in checking for structural serviceability. There is evidence from element tests that cyclic straining reduces or eliminates the swelling pressures that can otherwise be retained at zero effective vertical stress.

ACKNOWLEDGEMENT

The Authors are grateful for financial support of the Transport Research Laboratory, effected through a research contract placed with Cambridge University. The opinions expressed are, however, solely those of the Authors.

NOTATION

a, b equation (1) constants
c' true cohesion intercept
c_{mob} mobilized shear strength (also denoted by t)
c_s maximum shear stress t following strain
c_u undrained strength
E general point in the soil beneath the excavation
g gravitational acceleration
n model scale factor
OCR overconsolidation ratio ($\sigma'_{v\,max}/\sigma_v'$)
P prop force
Q toe force
R general point in the retained soil
s stress in plane strain
s' effective stress in plane strain
t shear stress in plane strain
u pore-water pressure
γ soil shear strain
Δu excess pore-water pressure
σ_h' effective horizontal stress
σ_v' effective vertical stress
ϕ secant angle of effective shearing resistance

Subscripts

av average
crit at a critical state
d after drainage
E relating to point beneath excavation
i initial, after excavation
max maximum
R relating to point in retained soil
s after swelling

REFERENCES

Al Tabbaa, A. (1988). *Permeability and stress–strain response of Speswhite kaolin.* PhD dissertation, University of Cambridge.

Amerasinge, S. F. (1973). *The stress–strain behaviour of clay at low stress levels and high over-consolidation ratios.* PhD dissertation, University of Cambridge.

Avgherinos, P. J. (1969). *Centrifuge testing of models made of soil.* PhD dissertation, University of Cambridge.

Bolton, M. D., Britto, A. M., Powrie, W. & White, T. P. (1989). Finite element analysis of a centrifuge model of a retaining wall embedded in overconsolidated clay. *Comput. Geotech.* **7,** 289–318.

Bolton, M. D. & Powrie, W. (1988). The behaviour of diaphragm walls in clay prior to collapse. *Géotechnique* **38,** No. 2, 167–189.

Bolton, M. D., Powrie, W. & Stewart, D. I. (1987). Effects on diaphragm walls of groundwater pressure rising in clays. *Proc. 9th Eur. Conf. Soil Mech., Dublin,* 759–762.

Bolton, M. D., Powrie, W. & Symons, I. F. (1990). *The design of stiff in-situ walls retaining overconsolidated clay.* Contractor report 199, Crowthorne: Transport and Road Research Laboratory.

Brooker, E. W. & Ireland, H. O. (1965). Earth pressures at rest related to stress history. *Can. Geotech. J.* **2,** No. 1, 1–15.

Burland, J. B. & Fourie, A. B. (1985). Testing of soils under conditions of passive stress relief. *Géotechnique* **35,** No. 2, 193–198.

Hubbard, H. W., Potts, D. M., Miller, D. & Burland, J. B. (1984). Design of the retaining walls for the M25 cut and cover tunnel at Bell Common. *Géotechnique* **34,** No. 4, 495–512.

Jardine, R. J., Potts, D. M., Fourie, A. B. & Burland, J. B. (1986). Studies of the influence of stress–strain characteristics in soil structure interaction. *Géotechnique* **36,** No. 3, 377–396.

Mair, R. J. (1979). *Centrifuge modelling of tunnel construction in soft clay.* PhD dissertation, University of Cambridge.

Milligan, G. W. E. & Bransby, P. L. (1976). Combined active and passive rotational failure of a retaining wall in sand. *Géotechnique* **26,** No. 3, 473–494.

Padfield, C. J. & Mair, R. J. (1984). *Design of retaining walls embedded in stiff clay.* Report 104. London: Construction Industry Research and Information Association.

Phillips, R. (1986). *Ground deformation in the vicinity of a trench heading.* PhD dissertation, University of Cambridge.

Powrie, W. (1985). Discussion on Performance of propped and cantilevered rigid walls. *Géotechnique* **35,** No. 4, 346–348.

Powrie, W. (1986). *The behaviour of diaphragm walls in clay.* PhD dissertation, University of Cambridge.

Schmidt, B. (1966). Discussion on Earth pressures at rest related to stress history, by Brooker and Ireland. *Can. Geotech. J.* **3,** No. 4, 239–242.

Schofield, A. N. (1980). The Rankine Lecture: Cambridge geotechnical centrifuge operations. *Géotechnique* **30,** No. 3, 227–267.

Simpson, B., Blower, T., Craig, R. N. & Wilkinson, W. B. (1989). *The engineering implications of rising groundwater levels in the deep aquifer beneath London.* Special publication 69. London: Construction Industry Research and Information Association.

Stewart, D. I. (1990). *Groundwater effects on in-situ walls in stiff clay.* PhD dissertation, University of Cambridge.

Tedd, P., Chard, B. M., Charles, J. A. & Symons, I. F. (1984). Behaviour of a propped embedded retaining wall in stiff clay at Bell Common tunnel. *Géotechnique* **34,** No. 4, 513–532.

Wroth, C. P. (1972). General theories of earth pressure and deformations. *Proc. 5th Eur. Conf. Soil Mech., Madrid* **2,** 33–52.

Wroth, C. P. (1975). In-situ measurement of initial stresses and deformation characteristics. *Proc. Specialty Conf. In-situ Measurement of Soil Properties, Raleigh,* 181–230.

Wroth, C. P. (1984). The interpretation of in-situ soil tests. *Géotechnique* **34,** No. 4, 449–489.